Hybrid Dual and NPC Six-Phase Drive Systems

Victor Felipe Moura Bezerra Melo, *Student Member, IEEE*, Cursino Brandão Jacobina, *Fellow, IEEE*, Nady Rocha, *Member, IEEE*, Reuben Palmer Rezende de Sousa, *Student Member, IEEE*, and Edgar Roosevelt Braga-Filho

***Abstract*—This paper presents two hybrid six-phase machine drive systems. The topologies are considered to be hybrid because two three-phase groups of the machine are fed by different types of converters. The purpose of these topologies is to be alternative configurations, being midway between the conventional six-leg two-level (2L) inverter, composed of 12 switches, and more complex structures, such as the six-leg three-level neutral point clamped (3L-NPC) inverter, composed of 24 switches and 12 clamping diodes, or the conventional 12-leg dual inverter, composed of 24 switches. One of the hybrid topologies is composed of 18 switches and the other is composed of 18 switches and 6 clamping diodes. A comparative study of harmonic distortion, semiconductor losses, and machine torque ripple is performed. Compared with the conventional 2L inverter, the proposed systems provide better performance in terms of harmonic distortion, overall semiconductor losses, and machine torque ripple and are less complex than dual and NPC inverters. Pulse width modulation (PWM) strategy is discussed and simulated. A modification in PWM strategy of the hybrid configurations is performed in order to obtain similar torque ripple to the cases when dual and 3L-NPC converters are used, even with lower number of semiconductor devices. Experimental results are also presented in order to validate the PWM strategy.**

***Index Terms*—AC motor drives, hybrid inverters, six-phase machine.**

I. Introduction

In THE 1920s, the concept of multiphase machines was created. They were first used with the objective of splitting the current per phase in order to obtain same machine power with lower current values. It was due to the fact that the circuit breakers at that time did not tolerate high current values in high power generation systems [1]. In the 1990s, the attention was once again turned to the multiphase machines, especially in transportation applications such as electric ship propulsion, due to their advantages when compared to three-phase machines, such as: 1) reduced current processed by each leg of the converter; 2) lower torque pulsations; 3) reduced rotor harmonic currents for induction motor drives, for the same machine volume; 4) reduced harmonic content of the dc-link current; 5) fault tolerance capability; and 6) the possibility of eliminating the common-mode voltage [2]–[4].

Nowadays, because of the aforementioned features and their reliability and size, these machines are used in aerospace, wind energy, and high-power industrial applications, among others.

On the other hand, multilevel converters, compared to the two-level (2L) one [see Fig. 1(a)], present several advantages such as: 1) enhanced quality of the output voltage at low switching frequencies; 2) low electromagnetic interference; 3) low voltage stress on semiconductor switches; 4) reduced dv/dt; 5) reduced common-mode voltage; 6) higher efficiency, etc [5].

In this context, the three-level neutral point clamped (3L-NPC) converter emerged in the early 1980's [6] and is considered the first multilevel power converter for medium-voltage applications [7]. Its application as a six-phase machine drive converter is illustrated in Fig. 1(b).

Also, an interesting type of cascaded multilevel converter, known as dual converter, was first proposed in [8] and has been widely employed in multiphase drive systems for five- [9], six- [10], and seven-phase machines [11]. It consists in cascading two converters, with one at each side of the load or machine windings, in an open-end winding (OEW) arrangement, as illustrated in Fig. 1(c) for a six-phase machine. This kind of structure may use single dc-link supply, but the use of separated dc-links permits the generation of voltages with higher number of steps and less harmonic distortion, mainly with unequal dc-link voltages. Also, by using separated dc-links, there is no zero-sequence current.

Knowing that a six-phase machine is composed of two three-phase groups, in this paper it is assumed that one group is composed of phases 1, 3, and 5 and is named as odd group and the other group is composed of phases 2, 4, and 6 and is named as even group. The machine used for simulation and experimental analysis is an asymmetrical squirrel-cage induction machine, meaning that the spatial shift between the two groups is of 30°.

In this way, by using conventional 2L, dual, and 3L-NPC converters, it is possible to feed each group by a different type of converter, which leads to hybrid configurations of Fig. 2.

Manuscript received October 7, 2016; accepted December 2, 2016. Date of publication December 20, 2016; date of current version June 23, 2017. Recommended for publication by Associate Editor A. Muetze.

V. F. M. B. Melo is with the Department of Electrical Engineering, COPELE, Federal University of Campina Grande, Campina Grande 58429-900, Brazil, and also with the Federal Institute of Technology of Pernambuco, Afogados da Ingazeira 56800-000, Brazil (e-mail: victor.melo@ee.ufcg.edu.br).

C. B. Jacobina and E. R. Braga-Filho are with the Federal University of Campina Grande, Campina Grande 58429-900, Brazil (e-mail: jacobina@dee.ufcg.edu.br; edgar@dee.ufcg.edu.br).

N. Rocha is with the Federal University of Paraíba, João Pessoa 58051-900, Brazil (e-mail: nadyrocha@cear.ufpb.br).

R. P. R. Sousa is with the Department of Electrical Engineering, COPELE, Federal University of Campina Grande, Campina Grande 58429-900, Brazil (e-mail: reubenpalmer@gmail.com).

Color versions of one or more of the figures in this paper are available online at http://ieeexplore.ieee.org.

Digital Object Identifier 10.1109/TPEL.2016.2641987

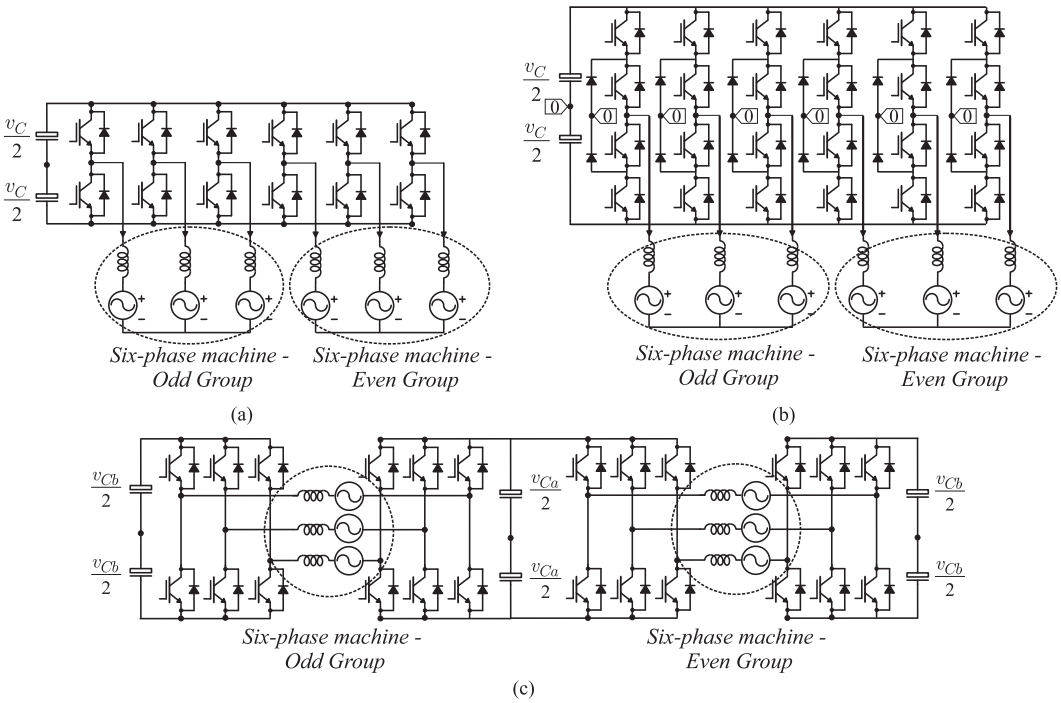

Fig. 1. Conventional configurations. (a) 2L converter. (b) 3L-NPC converter. (c) Dual converter.

In the first hybrid configuration (hybrid 1), the odd group is connected to a 2L converter and the even group is connected in an OEW arrangement to a three-phase dual converter [see Fig. 2(a)]. In the second hybrid configuration (hybrid 2), the odd group is connected to a 2L converter (identically to the first configuration) and the even group is connected to a 3L-NPC converter [see Fig. 2(b)].

These topologies present the advantages of: 1) having lower cost than that of dual and 3L-NPC converters due to the use of a lower number of insulated gated bipolar transistor (IGBT) devices; 2) low torque ripple, similar to the one obtained with dual and 3L-NPC converters; 3) reduced overall semiconductor losses and harmonic distortion in comparison to 2L converter.

Concerning the number of semiconductor devices, Table I shows how many devices are used by each topology.

Note that dual and 3L-NPC converters present 24 IGBT switches, which is the double of the number of switches used by 2L converter, which may represent high initial cost to set up these multilevel converters. Besides, 3L-NPC converter makes use of 12 clamping diodes, increasing the expense even more. On the other hand, topology hybrid 1 makes use of 18 IGBT switches and topology hybrid 2 is composed of the same number of switches as hybrid 1, but also of additional 6 clamping diodes. Nevertheless, topology hybrid 2 turns out to have lower initial cost than the dual inverter, even with the same number of semiconductor devices, because four 2L modules are more expensive than one 2L module plus one 3L-NPC module for similar rated voltage and current. In this way, the purpose of these topologies is to be alternative configurations, being midway between the conventional 2L one of Fig. 1(a) and the conventional multilevel ones of Fig. 1(b) and (c) in terms of complexity and number of components, with simplified gate drive circuitry, but also keeping the low torque ripple observed when multilevel converters are used.

In this paper, converters model and pulse width modulation (PWM) strategy for topologies hybrid 1 and 2 are presented. Besides, quantitative comparisons of harmonic distortion, semiconductor losses and machine torque ripple provided by conventional structures of Fig. 1 and the hybrid ones of Fig. 2 are performed in simulation. A method to reduce the machine torque ripple provided by the hybrid topologies is discussed and its validity is proven by means of simulations and experiments.

A version of this paper was presented in [12]. However, an additional discussion is added in the present paper, concerning the machine torque ripple provided by conventional and studied topologies. This additional information is discussed in Section VI. Also, a modification in the PWM strategy is performed in order to reduce the machine torque ripple for both hybrid topologies. With this modification, even with a lower number of semiconductor devices, it is possible to provide a torque ripple as low as the one obtained with dual and 3L-NPC converters. The present paper presents new simulation and experimental results by using an asymmetrical induction six-phase machine.

II. Converters Model

For configuration hybrid 1, the system is composed of a conventional three-leg converter (named inverter Ts) connected to the machine odd group and a conventional dual converter (inverters As and Bs) connected to the machine even group. In this way, voltages across odd and even phases are given by

$$v_{sk} = v_{stk0_t} - v_{s0_t} \tag{1}$$

$$v_{sj} = v_{saj0_a} - v_{sbj0_b} - v_{0_b0_a} \tag{2}$$

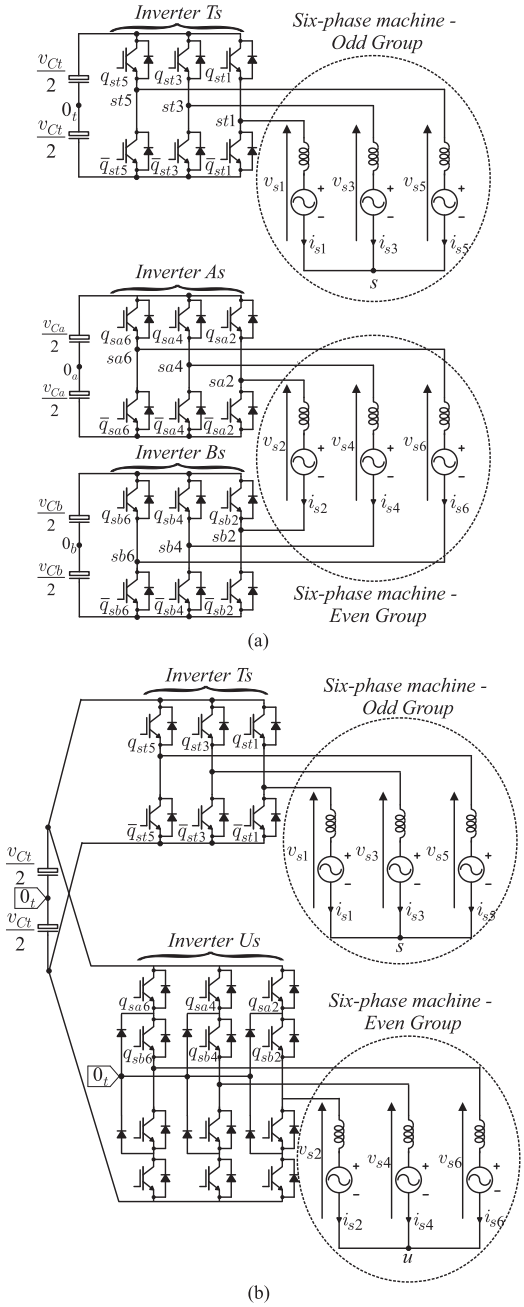

Fig. 2. Hybrid configurations. (a) Hybrid 1. (b) Hybrid 2.

where $k = 1, 3, 5$ and $j = 2, 4, 6$, v_{s0_t} is the voltage between the machine odd group Y-connection neutral point s and the dc-link midpoint 0_t of inverter Ts and $v_{0_b 0_a}$ is the voltage between the dc-link midpoints 0_b and 0_a.

Considering a balanced machine

$$v_{s0_t} = \frac{1}{3} \sum_{k=1,3,5} v_{stk0_t} \tag{3}$$

$$v_{0_b 0_a} = \frac{1}{3} \left(\sum_{j=2,4,6} v_{saj0_a} - \sum_{j=2,4,6} v_{sbj0_b} \right). \tag{4}$$

TABLE I
NUMBER OF SEMICONDUCTOR DEVICES FOR EACH TOPOLOGY

Topologies	IGBTs	Clamping diodes	Total
2L inverter [see Fig. 1(a)]	–	–	–
3L-NPC inverter [see Fig. 1(b)]	24	12	36
Dual inverter [see Fig. 1(c)]	24	–	24
Configuration hybrid 1 [see Fig. 2(a)]	18	–	18
Configuration hybrid 2 [see Fig. 2(b)]	18	6	24

Now, for topology hybrid 2, machine even group is connected to a 3L-NPC converter (named inverter Us). In this way, for the even group of topology hybrid 2

$$v_{sj} = v_{suj0_t} - v_{u0_t} \tag{5}$$

where v_{u0_t} is the voltage between the machine even group Y-connection neutral point u and the dc-link midpoint 0_t of inverter Us.

Considering a balanced machine

$$v_{u0_t} = \frac{1}{3} \sum_{j=2,4,6} v_{suj0_t}. \tag{6}$$

III. PWM STRATEGY

The PWM strategy has the purpose of determining the reference voltages of the inverters. These voltages are therefore compared to triangular carriers, and the gating signals are then obtained.

A. Odd Group—Configurations Hybrid 1 and Hybrid 2

Since the control system provides four reference voltages [v^*_{s1}, v^*_{s2}, v^*_{s3}, v^*_{s4} (the other two voltages are obtained from these)], for the odd group, it is necessary to obtain the reference pole voltages considering that

$$v^*_{sk} = v^*_{stk0_t} - v^*_{s0_t} \tag{7}$$

where $v^*_{s0_t}$ is the reference voltage between point s and midpoint 0_t of the inverter Ts. Then, the reference pole voltages of inverter Ts are given by

$$v^*_{stk0_t} = v^*_{sk} + v^*_{s0_t}. \tag{8}$$

In order to respect the dc-link voltage limits

$$v^*_{s0_t} = \mu_{s0_t} V^*_{s0_t \max} + (1 - \mu_{s0_t}) V^*_{s0_t \min} \tag{9}$$

where $0 \le \mu_{s0_t} \le 1$ and $V^*_{s0_t \max} = v_{Ct}/2 - \max\{v^*_{s1}, v^*_{s3}, v^*_{s5}\}$ and $V^*_{s0_t \min} = -v_{Ct}/2 - \min\{v^*_{s1}, v^*_{s3}, v^*_{s5}\}$. The reference pole voltages are valid for configurations hybrid 1 and hybrid 2.

B. Even Group—Configuration Hybrid 1

For the even group, introducing variables v^*_{srj}, it is possible to derive that

$$v^*_{srj} = v^*_{sj} + v^*_{0_b 0_a} \tag{10}$$

since $v^*_{srj} = v^*_{saj0_a} - v^*_{sbj0_b}$. In order to respect dc-link voltage limits, $v^*_{0_b 0_a}$ may be normalized making use of distribution

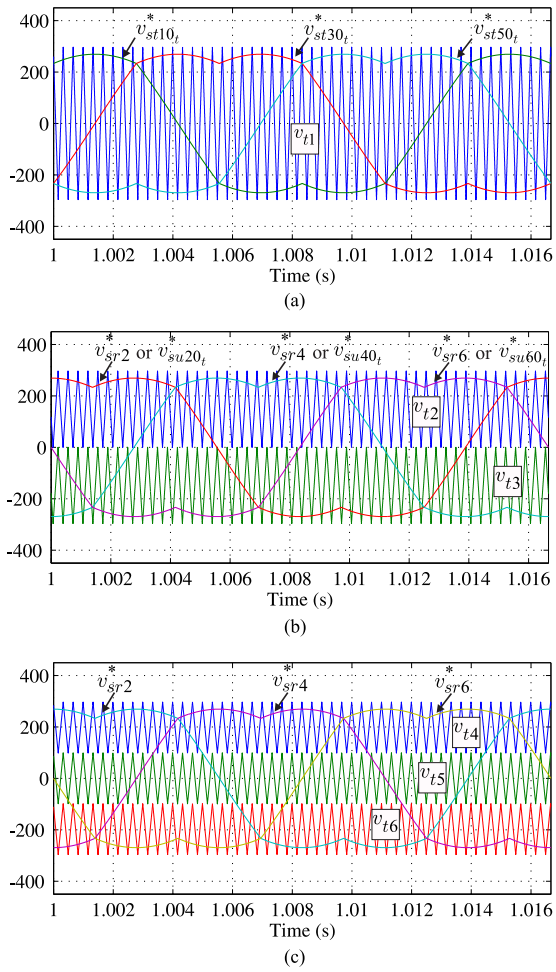

Fig. 3. Reference voltages and triangular carriers. (a) Inverter Ts for both hybrid topologies. (b) Inverters As and Bs for topology hybrid 1 with $v_{Ca} = v_{Cb}$ or inverter Us for topology hybrid 2. (c) Inverters As and Bs for topology hybrid 1 with $v_{Ca} = 2v_{Cb}$.

variable $\mu_{0_b 0_a}$ as follows:

$$v^*_{0_b 0_a} = \mu_{0_b 0_a} V^*_{0_b 0_a \max} + (1 - \mu_{0_b 0_a}) V^*_{0_b 0_a \min} \tag{11}$$

where $0 \le \mu_{0_b 0_a} \le 1$, $V^*_{0_b 0_a \max} = v_{Cab}/2 - \max\{v^*_{s2}, v^*_{s4}, v^*_{s6}\}$ and $V^*_{0_b 0_a \min} = -v_{Cab}/2 - \min\{v^*_{s2}, v^*_{s4}, v^*_{s6}\}$ and $v^*_{Cab} = v^*_{Ca} + v^*_{Cb}$.

Voltages v^*_{srj} are compared to level-shifted carriers accordingly to the level shift PWM (LS-PWM), widely discussed in the literature [13]–[15], aiming the generation of voltages with a higher number of steps, reducing harmonic distortion and dv/dt.

Fig. 3(a) brings the triangular carrier and the reference voltages used to determine the states of switches q_{st1}, q_{st3}, and q_{st5} of inverter Ts connected to the machine odd group in both hybrid topologies. Triangular carrier v_{t1} is compared to reference pole voltages $v^*_{stk0_t}$. Fig. 3(b) illustrates the reference voltages v^*_{srj} that are compared to triangular carriers v_{t2} and v_{t3} to determine the gating signals of inverters As and Bs with $v_{Ca} = v_{Cb}$. At last, for the case in which $v_{Ca} = 2v_{Cb}$, Fig. 3(c) illustrates the reference voltages v^*_{srj} that are compared to carriers v_{t4}, v_{t5}, and v_{t6} in order to determine inverters As and Bs gating signals. It is important to point out that all triangular carriers are synchronized, i.e., with no phase shift between them.

C. Even Group—Configuration Hybrid 2

For configuration hybrid 2, the PWM strategy is the same for both 2L and 3L-NPC inverters in terms of reference pole voltages. The difference is that the reference pole voltages of the 2L inverter are compared to one single triangular carrier and the reference pole voltages of the 3L-NPC inverter are compared to two level-shifted triangular carriers. In this way, the reference pole voltages of inverter Us are given by

$$v^*_{suj0_t} = v^*_{sj} + v^*_{u0_t} \tag{12}$$

where $v^*_{u0_t}$ is the reference voltage between the neutral point u and midpoint 0_t. In order to take into account the dc-link voltage limits

$$v^*_{u0_t} = \mu_{u0_t} V^*_{u0_t \max} + (1 - \mu_{u0_t}) V^*_{u0_t \min} \tag{13}$$

where $0 \le \mu_{u0_t} \le 1$ and $V^*_{u0_t \max} = v_{Ct}/2 - \max\{v^*_{s2}, v^*_{s4}, v^*_{s6}\}$ and $V^*_{u0_t \min} = -v_{Ct}/2 - \min\{v^*_{s2}, v^*_{s4}, v^*_{s6}\}$.

In this case, Fig. 3(b) illustrates reference voltages $v^*_{suj0_t}$ that are compared to carriers v_{t2} and v_{t3} in order to determine inverter Us gating signals.

IV. Harmonic Distortion

The harmonic distortion is calculated as shown in [12] by using the weighted total harmonic distortion (WTHD) of the machine phase voltages generated by the converters. In this section, a harmonic distortion comparison among the conventional 2L, 3L-NPC, and the dual inverters is performed. Note that the studied configurations are based on these types of inverters.

For this harmonic distortion analysis, the number of considered harmonics is $N_h = 500$ and generated voltages have amplitude of $V_s = 311$ V. Also, $\mu_{s0_t} = \mu_{0_b 0_a} = \mu_{u0_t} = 0.5$. DC-link voltage of conventional 2L and 3L-NPC inverters is made $v_C = 1.1 \times 311\sqrt{3} = 592.53$ V. Conventional dual inverter may operate under two different dc-link voltages conditions: 1) $v_{Ca} = v_{Cb} = v_C/2 = 296.27$ V or 2) $v_{Ca} = 2v_C/3 = 395.02$ V and $v_{Cb} = v_{Ca}/2 = 197.51$ V. This second combination is the best one in terms of harmonic distortion. In this way, dc-link voltages of the configuration hybrid 1 is $v_{Ct} = 592.53$ V and $v_{Ca} = v_{Cb} = 296.27$ V or $v_{Ca} = 2v_{Ct}/3 = 395.02$ V and $v_{Cb} = v_{Ca}/2 = 197.51$ V. For configuration hybrid 2, $v_{Ct} = 592.53$ V. Sampling frequency is 3 kHz.

Fig. 4 illustrates the machine phase voltages generated by 2L, 3L-NPC, and dual inverters. Fig. 4(a) shows the 2L inverter machine voltage waveform that is the same as odd group voltages waveform for configurations hybrid 1 and hybrid 2. Fig. 4(b) brings the dual and 3L-NPC inverters voltage waveform that is the same as even group voltages waveform for configuration hybrid 1 when $v_{Ca} = v_{Cb}$ and configuration hybrid 2. Fig. 4(c) illustrates dual inverter voltage waveform that is the same as even group voltages waveform for configuration hybrid 1 when $v_{Ca} = 2v_{Cb}$. It is noticeable that even group voltages for configuration hybrid 1 with $v_{Ca} = 2v_{Cb}$ have more steps than the

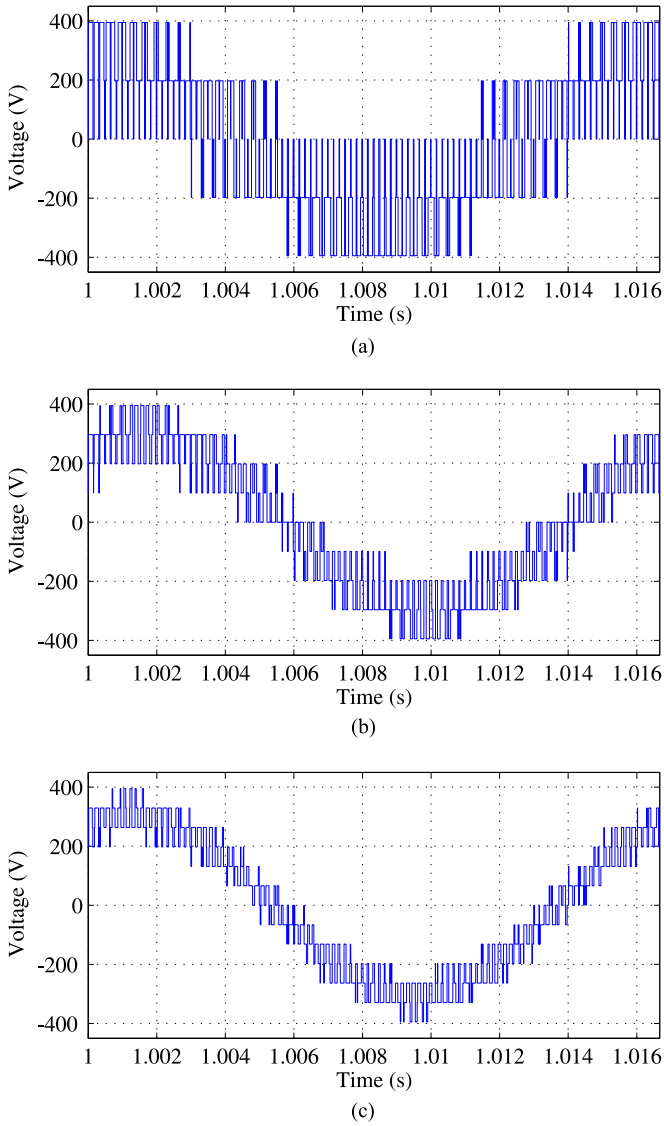

Fig. 4. Machine voltage waveform generated by the converters. (a) Odd group voltages waveform (hybrid 1 and hybrid 2). (b) Even group voltages waveform (hybrid 1 with $v_{Ca} = v_{Cb}$ and hybrid 2). (c) Even group voltages waveform (hybrid 1 with $v_{Ca} = 2v_{Cb}$).

TABLE II
WTHD VALUES FOR CONVENTIONAL SYSTEMS

Topologies	WTHD (%)
2L [see Fig. 1(a)]	0.78
3L-NPC [see Fig. 1(b)]	0.33
Dual inverter [see Fig. 1(c)] ($v_{Ca} = v_{Cb}$)	0.33
Dual inverter [see Fig. 1(c)] ($v_{Ca} = 2v_{Cb}$)	0.22

other configurations, characterizing the lowest harmonic distortion among them.

Table II shows the WTHD values obtained for 2L, 3L-NPC, and dual inverters. As expected, the studied inverters generate voltages with different harmonic distortion values for the machine odd and even groups. Odd group voltages of configurations hybrid 1 and hybrid 2 present the same WTHD value of the conventional 2L inverter. On the other hand, even group voltages of configuration hybrid 1 present the same WTHD values of conventional dual inverter for both dc-link values combinations. For configuration hybrid 2, even group voltages present the same WTHD of conventional 3L-NPC inverter.

Note that the even group voltages of configuration hybrid 1 for $v_{Ca} = 2v_{Cb}$ present the best harmonic distortion value, followed by the same configuration with $v_{Ca} = v_{Cb}$ and configuration hybrid 2.

TABLE III
SEMICONDUCTOR LOSSES FOR ALL TOPOLOGIES IN WATTS

Topologies	$P_{cond}(W)$	$P_{swit}(W)$	$P_{tot}(W)$
2L [see Fig. 1(a)]	4.63	49.53	54.16
3L-NPC [see Fig. 1(b)]	8.78	7.74	16.52
Dual inverter [see Fig. 1(c)] ($v_{Ca} = v_{Cb}$)	8.98	20.94	29.92
Dual inverter [see Fig. 1(c)] ($v_{Ca} = 2v_{Cb}$)	9.07	16.9	25.97
Conf. hybrid 1 [see Fig. 2(a)] ($v_{Ca} = v_{Cb}$)	6.81	35.24	42.05
Conf. hybrid 1 [see Fig. 2(a)] ($v_{Ca} = 2v_{Cb}$)	6.85	33.3	40.15
Conf. hybrid 2 [see Fig. 2(b)]	6.71	28.64	35.36

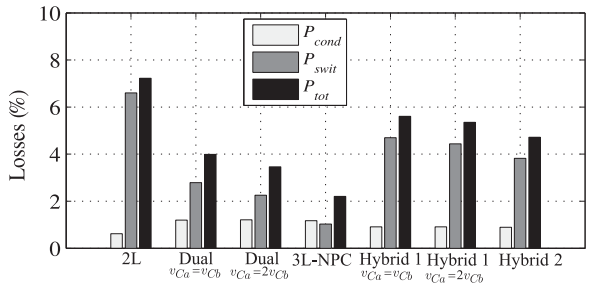

Fig. 5. Semiconductor losses for all topologies in percentage of machine power.

V. SEMICONDUCTOR LOSSES

The values of conduction and switching losses in the semiconductor devices that compose the converters are obtained by the method proposed in [16]. The switch loss model includes: 1) IGBT and diode conduction losses; 2) IGBT turn-ON losses; 3) IGBT turn-OFF losses; and 4) diode turn-OFF energy.

In this section, a semiconductor losses comparison between the conventional and studied configurations is performed. The conditions for this semiconductor losses analysis are the same as the ones for the harmonic distortion analysis, discussed in Section IV. The machine power is $P_M = 0.75$ kW.

Table III presents the values of power losses by conduction (P_{cond}), switching (P_{swit}), and total losses ($P_{tot} = P_{cond} + P_{swit}$) in watts for 2L, 3L-NPC, dual, and hybrid configurations. Fig. 5 shows the values of the power losses for the same topologies in percentage of the machine power.

As expected, configurations 3L-NPC, dual, and hybrid inverters permit the reduction of total losses when compared to configuration 2L. However, even though configurations 3L-NPC and dual present the lowest losses values among all structures, their initial cost is higher than that of configuration 2L, as aforementioned, since the number of switches doubles from

configuration 2L to configurations 3L-NPC and dual. In this way, if one does not want to have such high initial cost, the hybrid topologies discussed in this paper are midway between configuration 2L and configurations 3L-NPC and dual and may be interesting alternatives to reduce overall losses and switches voltage rating when compared to 2L inverter.

Note that, for the same number of switches, configuration hybrid 1 with $v_{Ca} = 2v_{Cb}$ presents virtually the same semiconductor losses as configuration hybrid 2, but provides even group voltages with less harmonic distortion. In this way, between the two proposed configurations, configuration hybrid 1 turns out to be better than configuration hybrid 2 when harmonic distortion and semiconductor losses are taken into account. Also, configuration hybrid 1 does not make use of additional clamping diodes, which is another advantage when compared to configuration hybrid 2.

VI. Torque Ripple

Another way of evaluating machine drive systems performance is observing the machine torque ripple. The torque ripple is intended to be as low as possible and is directly influenced by the inverter topology and by the PWM strategy. In fact, considering that high torque ripple increases the system vibrations and mechanical losses, it is very important drive topologies allied to suitable PWM strategies to have the reduction of torque ripple as one of their main goals. Assuming rotor flux reference frame and considering steady-state operation, the machine torque may be calculated as discussed in [17] as

$$T_e = p\frac{l_{sr}^2}{l_r} i_{sd}^r i_{sq}^r \tag{14}$$

where p is the number of pole pairs, l_{sr} is the equivalent stator–rotor mutual inductance, l_r is the rotor self-inductance and i_{sd}^r and i_{sq}^r are the stator direct and quadrature currents respectively.

Fig. 6 shows the machine torque and its frequency spectrum for all structures of this paper. The harmonics amplitudes are expressed in percentage of the torque fundamental dc value. The most significant machine torque harmonics oscillate in frequencies of 3, 6, 12, and 18 kHz, which are the sampling frequency, twice, four times, and six times the sampling frequency, respectively. As expected, hybrid configurations provide lower torque ripple than configuration 2L, but higher torque ripple than configurations 3L-NPC and dual, which can be also verified by observing the harmonics amplitudes. Configurations hybrid 1 and hybrid 2 manage to reduce the amplitude of these harmonics when compared to topology 2L. The lowest ripple is obtained with dual inverter with $v_{Ca} = 2v_{Cb}$, which has the lowest harmonics amplitudes among all topologies.

A. PWM Modification to Reduce Torque Ripple

It is known that machine torque waveform depend on the converter and on the PWM strategy. They determine the waveforms of voltages generated across the machine terminals, which in turn determine direct and quadrature voltages and currents, defining at last the machine torque. Direct and quadrature voltages are defined according to the space vector decomposition (SVD) technique first discussed in [18]. The used decoupling transformation matrix in the stationary reference frame for an asymmetrical six-phase machine is shown in [17].

In this way, v_{sd} and v_{sq} are

$$v_{sd} = \left[v_{s1} - \frac{v_{s3}}{2} - \frac{v_{s5}}{2} + v_{s2}\frac{\sqrt{3}}{2} - v_{s4}\frac{\sqrt{3}}{2}\right]/\sqrt{3} \tag{15}$$

$$v_{sq} = \left[\frac{\sqrt{3}v_{s3}}{2} - \frac{\sqrt{3}v_{s5}}{2} + \frac{v_{s2}}{2} + \frac{v_{s4}}{2} - v_{s6}\right]/\sqrt{3}. \tag{16}$$

Considering configurations hybrid 1 with $v_{Ca} = v_{Cb}$ and hybrid 2, Fig. 7(a) and (b) shows direct and quadrature voltages that generate the torque of Fig. 6(g). For topology hybrid 1 with $v_{Ca} = 2v_{Cb}$, Fig. 8(a) and (b) shows direct and quadrature voltages that generate the torque of Fig. 6(i).

However, it is possible to improve the torque ripple provided by the hybrid topologies. Since machine torque depends on direct and quadrature voltages, by improving them (reducing their dv/dt) the torque ripple may be reduced. For topology hybrid 1, this may be accomplished by slightly changing the instants, where IGBT switches of inverters As and Bs pulse. For topology hybrid 2, this is reached by slightly changing the instants where IGBT switches of the 3L-NPC converter pulse.

For example, consider Fig. 9(a), which illustrates phases 1 and 2 voltages during part of the 60-Hz machine cycle for configurations hybrid 1 with $v_{Ca} = v_{Cb}$ and hybrid 2. Note that most of the time when v_{s1} assumes a lower voltage level, so does v_{s2}. Also, when v_{s1} assumes a higher voltage level, so does v_{s2}. This effect is highlighted by shaded areas. The same happens for the other phases and during the whole 60-Hz cycle. As v_{sd} and v_{sq} waveforms are defined by stator voltages waveforms, when the pulses happen at the same time as shown, high dv/dt is observed in direct and quadrature voltages as can be seen in Fig. 9(b) and (c), which is obtained by zooming in on the shaded areas of Fig. 7(a) and (b), respectively.

Now, in order to change the instants where the pulses occur without affecting the waveforms of voltages across the machine terminals, it is necessary to slightly change the phase angle between triangular carriers, as illustrated in Fig. 10(a) for configuration hybrid 1 with $v_{Ca} = v_{Cb}$ and configuration hybrid 2. In this case, v_{t1} is 90° out-of-phase with triangulars v_{t2} and v_{t3}. By using these carriers, phases 1 and 2 voltages are generated as illustrated in Fig. 10(b). Note that most of the time when v_{s1} assumes lower voltage level, v_{s2} assumes a higher voltage level and vice-versa. This effect was highlighted by shaded areas. The same happens for the other phases and during the whole 60-Hz cycle. For this case, v_{sd} and v_{sq} waveforms are as shown in Fig. 10(c) and (d). Note lower dv/dt compared to the one observed in Fig. 9(b) and (c).

In this way, generated direct and quadrature voltages for the whole 60-Hz machine cycle are illustrated in Fig. 11(a) and (b) along with the machine torque and its frequency spectrum, which are illustrated in Fig. 11(c) and (d), respectively. Note a ripple reduction in comparison with torque of Fig. 6(g). The harmonics amplitudes are considerably reduced by using out-of-phase triangular carriers.

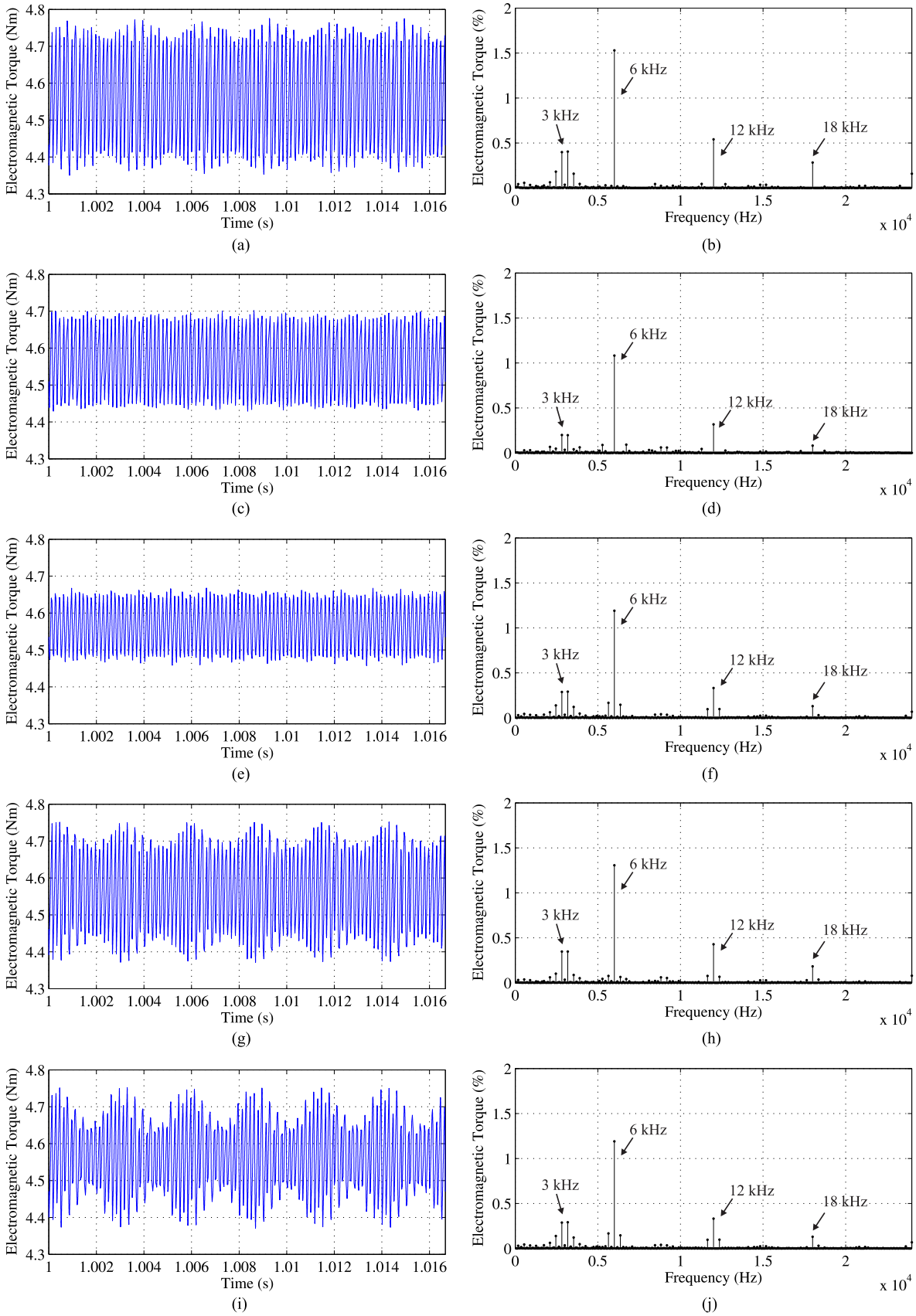

Fig. 6. Machine torque waveform and its frequency spectrum. (a) and (b) 2L. (c) and (d) Dual—$v_{Ca} = v_{Cb}$ and 3L-NPC. (e) and (f) Dual—$v_{Ca} = 2v_{Cb}$. (g) and (h) Hybrid 1—$v_{Ca} = v_{Cb}$ and hybrid 2. (i) and (j) Hybrid 1—$v_{Ca} = 2v_{Cb}$.

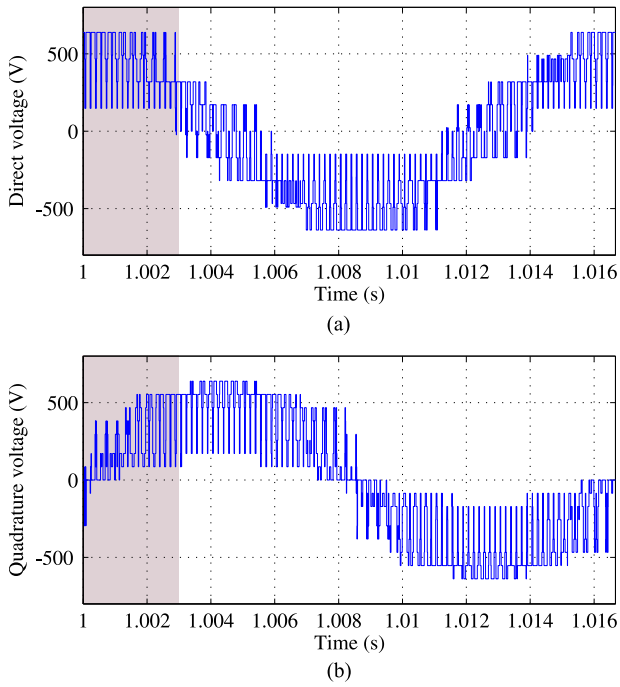

Fig. 7. Voltage waveforms for configuration hybrid 1 with $v_{Ca} = v_{Cb}$ and configuration hybrid 2 with synchronized carriers. (a) Direct voltage. (b) Quadrature voltage.

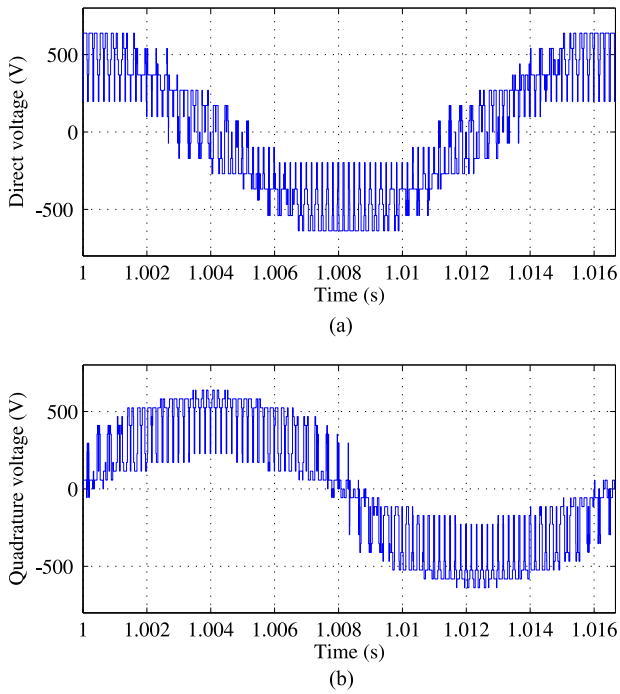

Fig. 8. Voltage waveforms for configuration hybrid 1 with $v_{Ca} = 2v_{Cb}$ with synchronized carriers. (a) Direct voltage. (b) Quadrature voltage.

Similarly, considering topology hybrid 1 with $v_{Ca} = 2v_{Cb}$, v_{t1} may be made 90° out-of-phase with triangulars v_{t4}, v_{t5}, and v_{t6}, as illustrated in Fig. 12(a). By using these carriers, generated direct and quadrature voltages are illustrated in Fig. 12(b) and (c) along with the machine torque and its frequency spectrum,

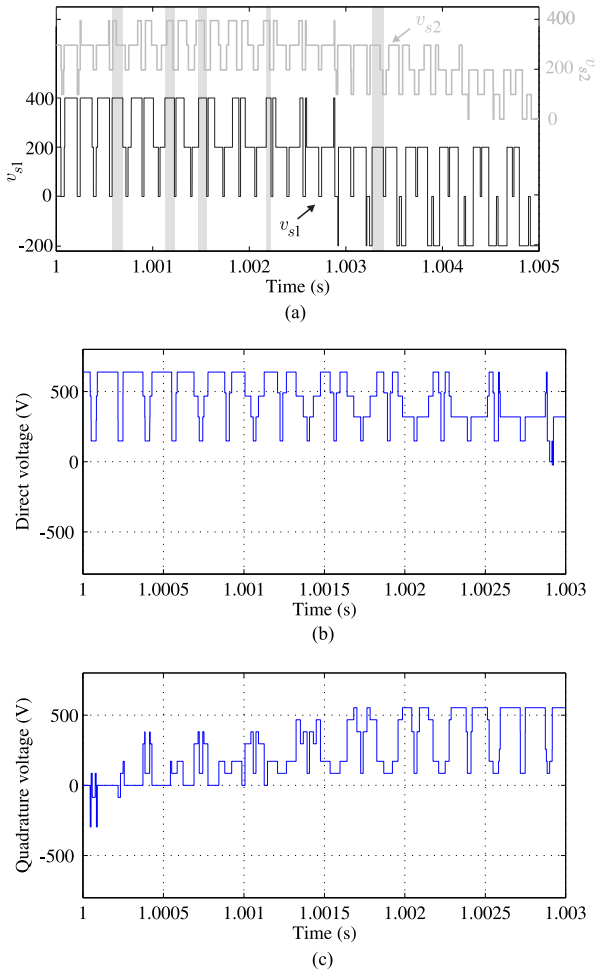

Fig. 9. Voltage waveforms for configuration hybrid 1 with $v_{Ca} = v_{Cb}$ and configuration hybrid 2 with synchronized carriers. (a) Phases 1 and 2 voltages. (b) Direct voltage. (c) Quadrature voltage.

TABLE IV
TORQUE RIPPLE IN PERCENTAGE OF FUNDAMENTAL DC VALUE

Topologies	Torque ripple (%)
2L [see Fig. 1(a)]	9.23
3L-NPC [see Fig. 1(b)]	5.86
Dual inverter [see Fig. 1(c)] ($v_{Ca} = v_{Cb}$)	5.86
Dual inverter [see Fig. 1(c)] ($v_{Ca} = 2v_{Cb}$)	4.2
Conf. hybrid 1 [see Fig. 2(a)] ($v_{Ca} = v_{Cb}$) with synchronized carriers	8.29
Conf. hybrid 1 [see Fig. 2(a)] ($v_{Ca} = v_{Cb}$) with shifted carriers	6.56
Conf. hybrid 1 [see Fig. 2(a)] ($v_{Ca} = 2v_{Cb}$) with synchronized carriers	8.29
Conf. hybrid 1 [see Fig. 2(a)] ($v_{Ca} = 2v_{Cb}$) with shifted carriers	5.47
Conf. hybrid 2 [see Fig. 2(b)] with synchronized carriers	8.29
Conf. hybrid 2 [see Fig. 2(b)] with shifted carriers	6.56

which are illustrated in Fig. 12(d) and (e), respectively. Note a ripple reduction in comparison with torque of Fig. 6(i).

Table IV brings the values of the torque ripple for all topologies in percentage of the fundamental dc value. Note that the lowest torque ripple is obtained with dual inverter with $v_{Ca} = 2v_{Cb}$.

However, when out-of-phase carriers are used, topology hybrid 1 with $v_{Ca} = 2v_{Cb}$ reduces significantly the machine

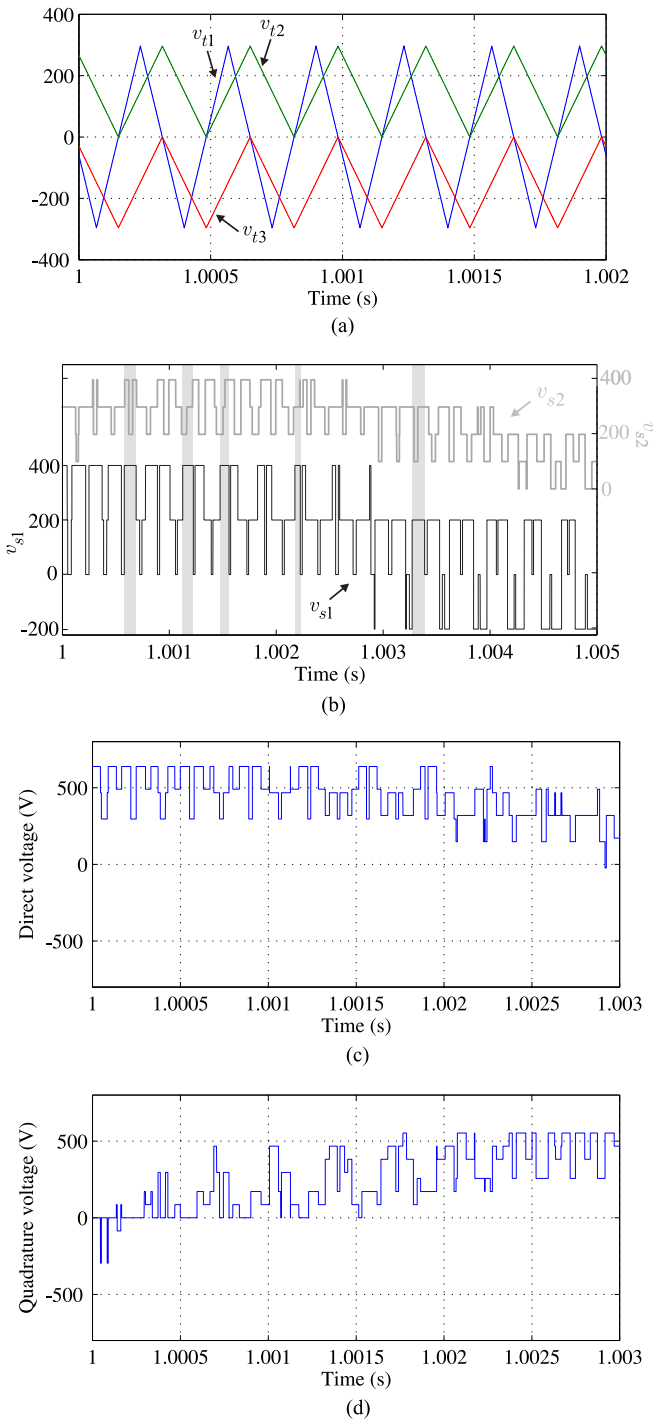

Fig. 10. Out-of-phase triangular carriers and voltage waveforms for configuration hybrid 1 with $v_{Ca} = v_{Cb}$ and configuration hybrid 2. (a) v_{t1}, v_{t2} and v_{t3}. (b) Phases 1 and 2 voltages. (c) Direct voltage. (d) Quadrature voltage.

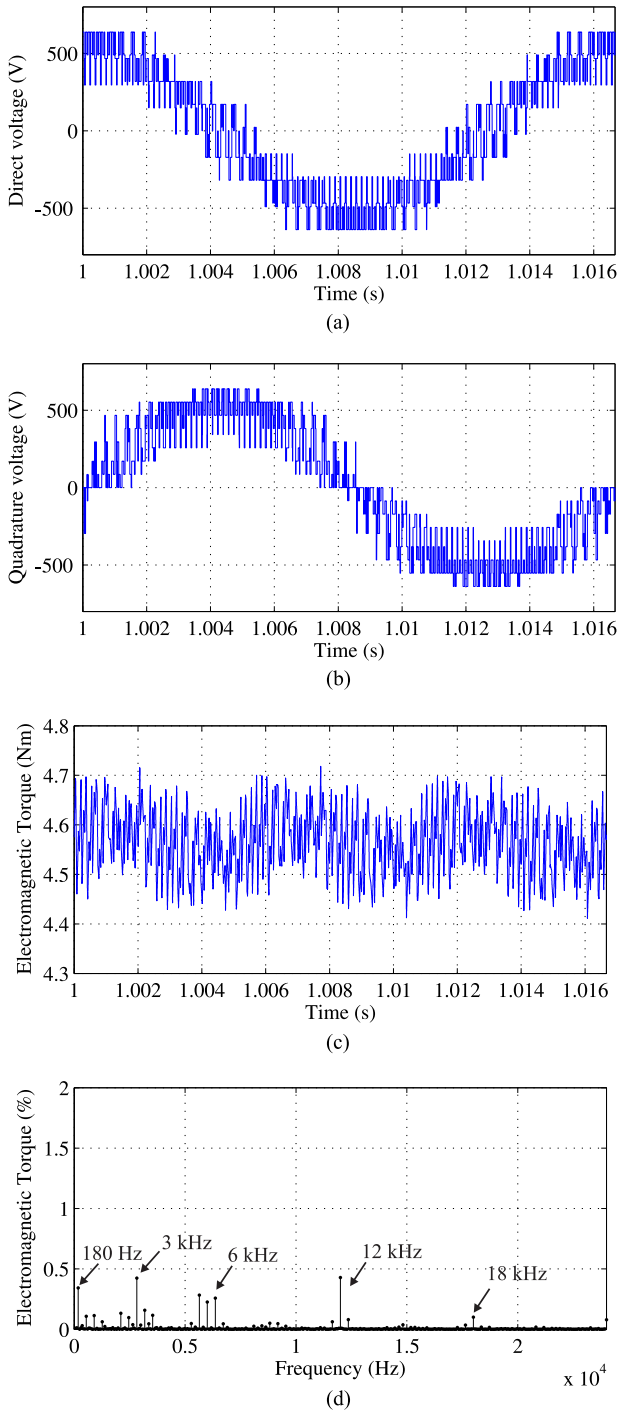

Fig. 11. Curves for configuration hybrid 1 with $v_{Ca} = v_{Cb}$ and configuration hybrid 2 with out-of-phase carriers. (a) Direct voltage. (b) Quadrature voltage. (c) Machine torque waveform. (d) Machine torque frequency spectrum.

torque ripple, which becomes lower than the one provided by dual inverter with $v_{Ca} = v_{Cb}$. Also, topology hybrid 2 reduces the provided torque ripple as well when out-of-phase carriers are used.

In this way, as can be seen in Table IV, it is possible to reduce the machine torque ripple using the hybrid topologies, which are composed of a lower number of semiconductor components than dual and 3L-NPC converters.

VII. Experimental Results

The experimental setup is based on converters composed of IGBTs from SEMIKRON controlled by a digital signal processor TMS320F28335 with a microcomputer equipped with appropriate plug-in boards and sensors. Also, an asymmetrical six-phase induction machine is mechanically coupled to a dc generator, which feeds resistive loads. DC generator plus resistive loads work as a mechanical load to the

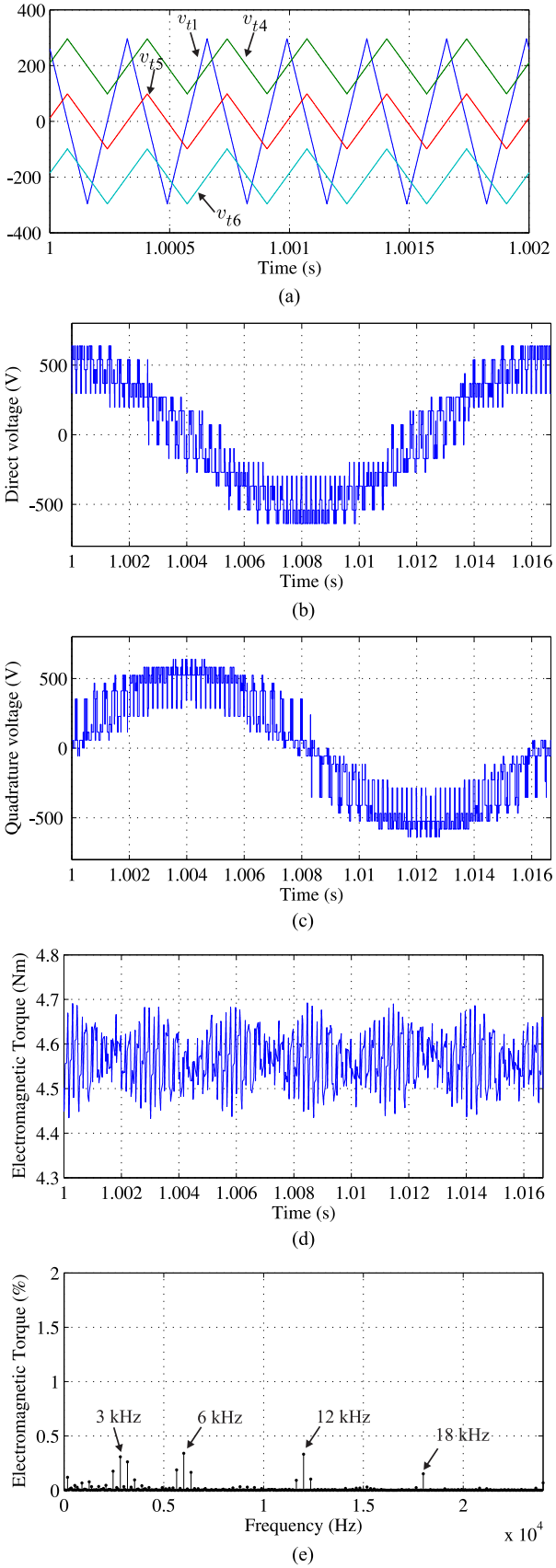

Fig. 12. Curves for configuration hybrid 1 with $v_{Ca} = 2v_{Cb}$ with out-of-phase carriers. (a) Triangular carriers. (b) Direct voltage. (c) Quadrature voltage. (d) Machine torque waveform. (e) Machine torque frequency spectrum.

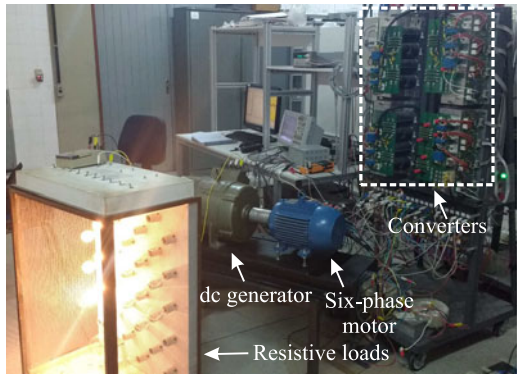

Fig. 13. Experimental setup.

TABLE V
SIX-PHASE INDUCTION MOTOR PARAMETERS

Parameters	Values
r_s	16.2 Ω
r_r	8.9 Ω
l_s	1.47 H
l_r	1.38 H
l_{sr}	1.38 H
l_{ls}	45 mH
Machine phase shift	30°
Rated voltage	220 V
Rated power	0.75 kW
Rated current	0.866 A
Frequency	60 Hz
Number of poles	4
Rated speed	1760 r/min

induction motor. The converters generate the voltages across the induction motor terminals. The photo of the experimental setup is shown in Fig. 13.

Motor parameters are shown in Table V. Experiments were performed under machine rated conditions. For configuration hybrid 1, dc-link voltages are $v_{Ct} = 592.53$ V and $v_{Ca} = v_{Cb} = v_{Ct}/2 = 296.27$ V. For configuration hybrid 2, $v_{Ct} = 592.53$ V. DC-link voltages are imposed by the grid by means of diode rectifiers and isolation transformers.

For configuration hybrid 1, Fig. 14(a) shows odd group currents and phase 1 voltage and Fig. 14(b) illustrates even group currents and phase 2 voltage. Note that these voltage waveforms are in full accordance with the ones shown in Fig. 4(a) and (b), validating the discussed PWM strategy. Knowing that from the measured stator currents it is possible to calculate i^r_{sd} and i^r_{sq} by means of the SVD technique, equation (14) may be used once again to calculate the machine electromagnetic torque. Therefore, from the measured stator currents, the machine electromagnetic torque was calculated.

In this way, Fig. 15(a) and (b) illustrates the machine electromagnetic torque waveforms when synchronized carriers and 90° out-of-phase carriers are utilized, respectively. Note the reduction in torque ripple by utilizing out-of-phase carriers, which validates the discussed PWM modification in order to reduce torque ripple explained in Section VI-A.

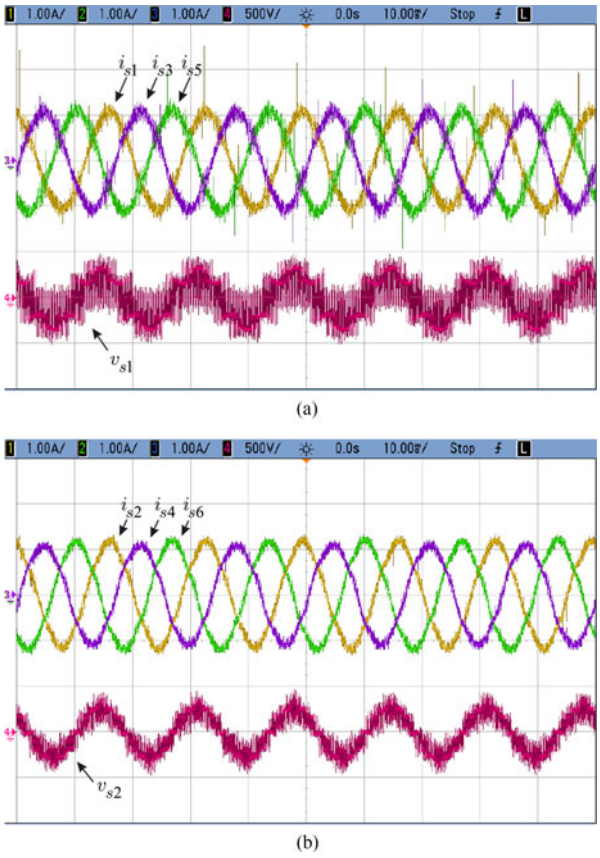

Fig. 14. Experimental results—configuration hybrid 1—machine currents and voltages. (a) Odd group currents and phase 1 voltage. (b) Even group currents and phase 2 voltage.

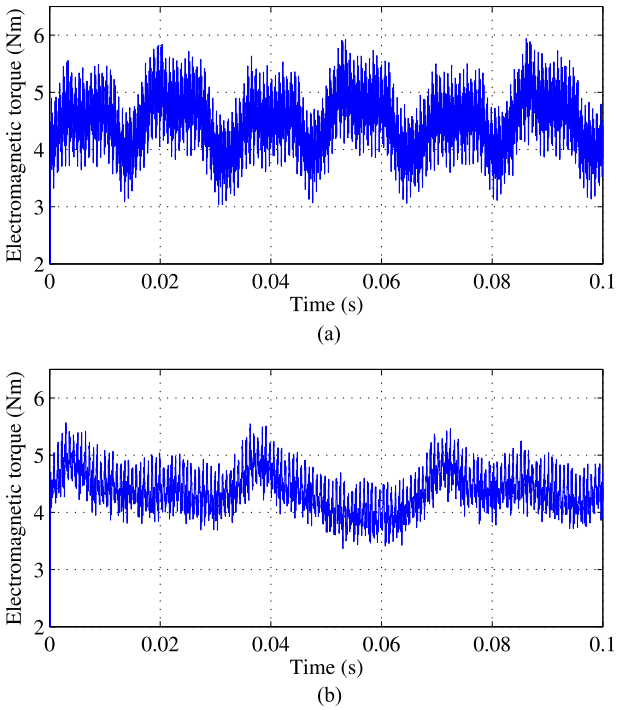

Fig. 15. Experimental results—configuration hybrid 1—machine electromagnetic torque. (a) With synchronized carriers. (b) With out-of-phase carriers.

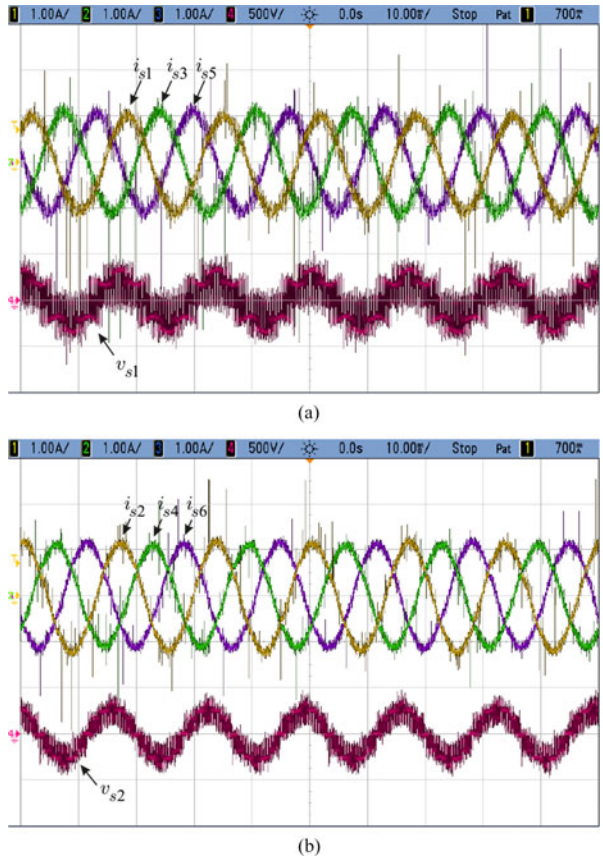

Fig. 16. Experimental results—configuration hybrid 2—machine currents and voltages. (a) Odd group currents and phase 1 voltage. (b) Even group currents and phase 2 voltage.

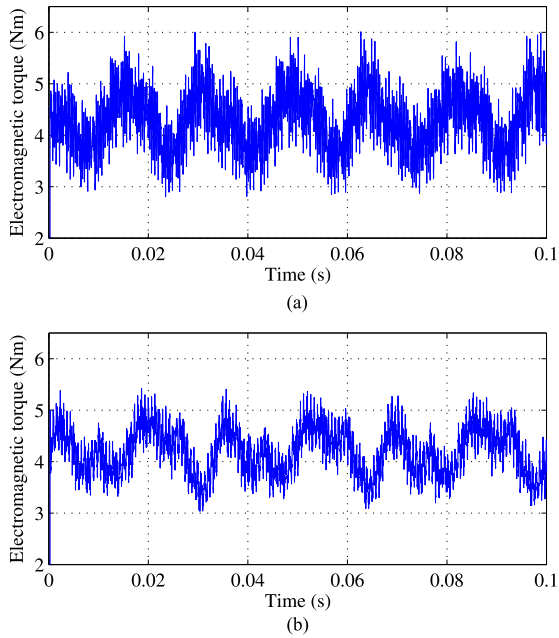

Fig. 17. Experimental results—configuration hybrid 2—machine electromagnetic torque. (a) With synchronized carriers. (b) With out-of-phase carriers.

Similarly for configuration hybrid 2, Fig. 16(a) shows odd group currents and phase 1 voltage and Fig. 16(b) illustrates even group currents and phase 2 voltage. Fig. 17(a) and (b) shows machine electromagnetic torque obtained with synchronized carriers and with out-of-phase carriers, respectively. Note the reduction of torque ripple by using out-of-phase carriers, validating the PWM modification to reduce torque ripple for this configuration as well.

VIII. Conclusion

In this paper, two hybrid drive topologies, which are midway between the conventional dual and 3L-NPC inverters and the conventional six-leg 2L inverter, were discussed. They provide better performance in terms of harmonic distortion, overall semiconductor losses, and machine torque ripple than conventional 2L inverter and are less complex than dual and 3L-NPC inverters. Besides, it was proven that the studied hybrid topologies may provide low torque ripple by phase shifting the carriers used for the definition of the gating signals. In this way, the hybrid configurations provide torque ripple as low as dual and 3L-NPC inverters, but employing a lower number of semiconductor devices. PWM strategies were discussed and simulations and experimental results were presented to validate these strategies.

References

[1] H. Kim, K. Shin, S. Englebretson, N. Frank, and W. Arshad, "Analytical model of multiphase permanent magnet synchronous machines for energy and transportation applications," in *Proc. 2013 IEEE Int. Elect. Mach. Drives Conf.*, May 2013, pp. 172–179.

[2] E. Levi, R. Bojoi, F. Profumo, H. Toliyat, and S. Williamson, "Multiphase induction motor drives a technology status review," *IET Elect. Power Appl.*, vol. 1, no. 4, pp. 489–516, 2007.

[3] E. Levi, "Multiphase electric machines for variable-speed applications," *IEEE Trans. Ind. Electron.*, vol. 55, no. 5, pp. 1893–1909, May 2008.

[4] E. Levi, "Advances in converter control and innovative exploitation of additional degrees of freedom for multiphase machines," *IEEE Trans. Ind. Electron.*, vol. 63, no. 1, pp. 433–448, Jan. 2016.

[5] P. P. Rajeevan, K. Sivakumar, K. Gopakumar, C. Patel, and H. Abu-Rub, "A nine-level inverter topology for medium-voltage induction motor drive with open-end stator winding," *IEEE Trans. Ind. Electron.*, vol. 60, no. 9, pp. 3627–3636, Sep. 2013.

[6] A. Nabae, I. Takahashi, and H. Akagi, "A new neutral-point-clamped PWM inverter," *IEEE Trans. Ind. Appl.*, vol. IA-17, no. 5, pp. 518–523, Sep. 1981.

[7] S. Kouro *et al.*, "Recent advances and industrial applications of multilevel converters," *IEEE Trans. Ind. Electron.*, vol. 57, no. 8, pp. 2553–2580, Aug. 2010.

[8] H. Stemmler and P. Guggenbach, "Configurations of high-power voltage source inverter drives," in *Proc. 5th Eur. Conf. Power Electron. Appl.*, vol. 5, 1993, pp. 7–14.

[9] M. Darijevic, M. Jones, and E. Levi, "An open-end winding four-level five-phase drive," *IEEE Trans. Ind. Electron.*, vol. 63, no. 1, pp. 538–549, Jan. 2016.

[10] F. Patkar, E. Levi, and M. Jones, "A six-phase multilevel space vector PWM algorithm for a dual-inverter supplied drive," in *Proc. 6th IET Int. Conf. Power Electron. Mach. Drives*, 2012, p. A133.

[11] N. Bodo, M. Jones, and E. Levi, "Multi-level space-vector PWM algorithm for seven-phase open-end winding drives," in *Proc. 2011 IEEE Int. Symp. Ind. Electron.*, Jun. 2011, pp. 1881–1886.

[12] V. F. M. B. Melo, C. B. Jacobina, and N. Rocha, "Hybrid open-end and NPC AC six-phase machine drive systems," in *Proc. IEEE Energy Convers. Congr. Expo.*, Sep. 2014, pp. 3872–3879.

[13] G. Carrara, S. Gardella, M. Marchesoni, R. Salutari, and G. Sciutto, "A new multilevel PWM method: A theoretical analysis," *IEEE Trans. Power Electron.*, vol. 7, no. 3, pp. 497–505, Jul.1992.

[14] M. Tamasas, M. Saleh, M. Shaker, and A. Hammoda, "Evaluation of modulation techniques for 5-level inverter based on multicarrier level shift PWM," in *Proc. Mediterranean Electrotech. Conf.*, Apr. 2014, pp. 17–23.

[15] T. V. V. S. Lakshmi, N. George, S. Umashankar, and D. P. Kothari, "Cascaded seven level inverter with reduced number of switches using level shifting PWM technique," in *Proc. 2013 Int. Conf. Power, Energy Control*, Feb. 2013, pp. 676–680.

[16] J. A. A. Dias, E. C. dos Santos, C. B. Jacobina, and E. R. C. da Silva, "Application of single-phase to three-phase converter motor drive systems with IGBT dual module losses reduction," in *Proc. 2009 Brazilian Power Electron. Conf.*, Sep. 2009, pp. 1155–1162.

[17] H. S. Che, M. J. Duran, E. Levi, M. Jones, W.-P. Hew, and N. A. Rahim, "Postfault operation of an asymmetrical six-phase induction machine with single and two isolated neutral points," *IEEE Trans. Power Electron.*, vol. 29, no. 10, pp. 5406–5416, Oct. 2014.

[18] T. Lipo, "Space vector PWM control of dual three-phase induction machine using vector space decomposition," *IEEE Trans. Ind. Appl.*, vol. 31, no. 5, pp. 1100–1109, Sep./Oct. 1995.

Victor Felipe Moura Bezerra Melo (S'13) was born in Pesqueira, Brazil, in 1988. He received the B.S. and M.S. degrees in electrical engineering from the Federal University of Campina Grande, Campina Grande, Brazil, in 2012 and 2013, respectively, where he is currently working toward the Ph.D. degree.

Since 2014, he has been with Federal Institute of Technology of Pernambuco, Afogados da Ingazeira, Brazil, where he is currently a Professor. His current research interests include power electronics, static converters, electrical drives, and active power filters.

Cursino Brandão Jacobina (S'78–M'78–SM'98–F'14) was born in Correntes, Brazil, in 1955. He received the B.S. degree in electrical engineering from the Federal University of Paraíba, Campina Grande, Brazil, in 1978 and the Diplôme d'Etudes Approfondies and the Ph.D. degrees in electrical engineering from the Institut National Polytechnique de Toulouse, Toulouse, France, in 1980 and 1983, respectively.

From 1978 to March 2002, he was with the Department of Electrical Engineering, Federal University of Paraíba, João Pessoa, Brazil. Since April 2002, he has been with the Department of Electrical Engineering, Federal University of Campina Grande, Campina Grande, where he is currently a Professor. His research interests include electrical drives, power electronics, and energy systems.

Nady Rocha (M'10) was born in São Gabriel, Brazil, in 1982. He received the B.S., M.S., and Ph.D. degrees in electrical engineering from the Federal University of Campina Grande, Campina Grande, Brazil, in 2006, 2008, and 2010, respectively.

Since 2011, he has been with the Department of Electrical Engineering, Federal University of Paraíba, João Pessoa, Brazil, where he is currently an Associate Professor of electrical engineering, and since 2013, he has been a tutor of the Tutorial Education Program. His research interests include power electronics, renewable energy sources, and electrical drives.

Reuben Palmer Rezende de Sousa (S'13) was born in Campina Grande, Brazil, in 1991. He received the B.S. and M.S. degrees in electrical engineering from the Federal University of Campina Grande, Campina Grande, Brazil, in 2014 and 2015, respectively, where he is currently working toward the Ph.D. degree.

Edgar Roosevelt Braga-Filho received the B.S. degree from Federal University of Paraíba, João Pessoa, Brazil, and the Doctoral degree from the Federal University of Campina Grande, Campina Grande, Brazil, both in electrical engineering.

He is currently a Faculty Member of the Department of Electrical Engineering, Federal University of Campina Grande. His research interests include the fields of electrical machines and drive systems.